

Topological Weyl-like Phonons and Nodal Line Phonons in Graphene

Jiangxu Li,^{1,2} Lei Wang,^{1,2} Jiayi Liu,^{1,2} Ronghan Li,¹ Zhenyu Zhang,³ and Xing-Qiu Chen^{1,*}

¹Shenyang National Laboratory for Materials Science, Institute of Metal Research,
Chinese Academy of Sciences, Shenyang 110016, China

²School of Materials Science and Engineering, University of Science and Technology of China, 110016 Shenyang, Liaoning, China

³International Center for Quantum Design of Functional Materials (ICQD),

Hefei National Laboratory for Physical Sciences at the Microscale,
and Synergetic Innovation Center of Quantum Information and Quantum Physics,
University of Science and Technology of China, Hefei, China

(Dated: March 22, 2022)

By means of first-principles calculations and modeling analysis, we have predicted that the traditional 2D-graphene hosts the topological phononic Weyl-like points (PWs) and phononic nodal line (PNL) in its phonon spectrum. The phonon dispersion of graphene hosts three type-I PWs (both PW1 and PW2 at the BZ corners K and K' , and PW3 locating along the Γ - K line), one type-II PW4 locating along the Γ - M line, and one PNL surrounding the centered Γ point in the $q_{x,y}$ plane. The calculations further reveal that Berry curvatures are vanishingly zero throughout the whole BZ, except for the positions of these four pairs of Weyl-like phonons, at which the non-zero singular Berry curvatures appear with the Berry phase of π or $-\pi$, confirming its topological non-trivial nature. The topologically protected non-trivial phononic edge states have been also evidenced along both the zigzag-edged and armchair-edged boundaries. These results would pave the ways for further studies of topological phononic properties of graphene, such as phononic destructive interference with a suppression of backscattering and intrinsic phononic quantum Hall-like effects.

Graphene, consisting of the one-atom-thick carbon in the two-dimensional hexagonal lattice, distinguishes itself as an ideal platform for various interesting and unusual properties, such as large, tunable carrier densities $n \sim 10^{11}$ - 10^{14} cm⁻², an ultrasmall, tunable Drude mass, and exceptionally long intrinsic relaxation times, and so on. These are mainly because its electronic structure can be described at low energies by a massless Dirac-Fermion model. On basis of graphene, Kane and Mele contributed a pioneered theoretical discovery to predict its quantum spin Hall effect with breaking the Dirac cone into a gap by forcing its spin-orbit coupling interaction [1], witnessing a new phase of quantum matter, lately called topological insulators in HgTe[2, 3], with insulating bulk and quantized and robust edge conductance. In parallel with electrons, still on basis of the structure of graphene the topological nature of the phonon Hall effect was theoretically proposed by interplaying Raman-type spin-phonon interaction [4] and the infrared topological plasmons was also recently proposed by breaking time-reversal symmetry under a static magnetic field [5]. The other two time-reversal-symmetry breaking two-dimensional systems were theoretically proposed to show topological phonon states with robust one-way elastic edge waves [6, 7], which immune to backscattering. Interesting, in all these studies [1, 4–7] the time-reversal-symmetry breaking fields by gyroscopic inertial effects [6, 7], spin-orbit coupling effects [1], spin-phonon interaction [4], and static magnetic field [5] are necessary to induce the topologically protected one-way electronic or phononic edge states on 2D systems. But, to date it has not been still clear whether or not the phonon spectrum of graphene itself is topological.

In Ref. [7], the modeling analysis for four phonon bands with the occurrence of the complete band gap for a hexagonal phononic crystal reveals that this gap is topologically trivial, since the time-reversal symmetry is not broken and

the Chern numbers of the bands are all zero. It was the reason as to why the authors introduced gyroscopic coupling to their modeling to obtain the non-trivial topological nature. In similarity to this work, in Ref. [8] various novel topological effects of phonons, including topologically protected pseudospin-polarized interface states and phonon pseudospin Hall effect, have been theoretically modeled in the Kekulé lattice. Returning to graphene, its unit cell has two carbon atoms allowing six degrees of freedom for atomic displacements. Even with the equal masses for two carbon atoms, it is possible to have intrinsically topologically protected phononic states in graphene because the extra two freedoms – vibration modes – along the direction normal to the xy plane, that definitely increases its perturbations. With such a purpose, we have revisited the issue of the phonon dispersions of graphene. Interestingly, we have found that the topology is the intrinsic property of the phonon spectrum for graphene. Our calculations reveals that, in the 2D hexagonal Brillouin zone (BZ), Weyl-like phonons not only exist at two inequivalent K and K' points but also appear on the Γ - L line and Γ - K line. Both of type-I and type-II Weyl-like phonons are found in the BZ. More interesting, there still exists a phononic nodal line (PNL) surrounding the centered Γ point. Furthermore, we have evidenced the non-trivial edge states along both zigzag-edged and armchair-edged boundaries, which are indeed confined to the boundaries in one-way propagation.

Based on the density functional theory(DFT) [9, 10] and density functional perturbation theory(DFPT) [11], we have calculated the stable lattice constants and the phonon dispersion. Both DFT and DFPT calculations have been performed by the Vienna *ab initio* Simulation Package (VASP) [12–14]. We adopted the projector augmented wave (PAW) [15, 16] potentials and the generalized gradient approximation (GGA) within the Perdew-Burke- Ernzerhof (PBE) exchange-

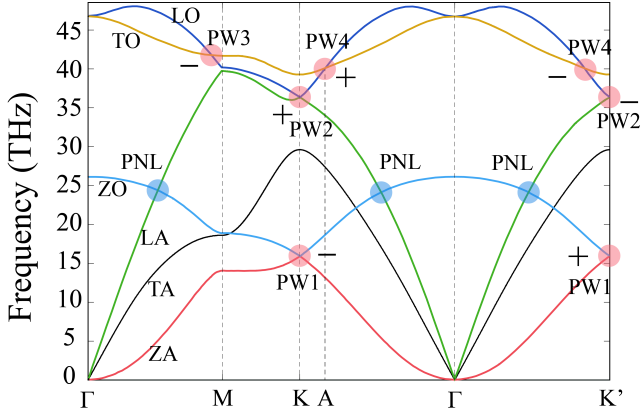


FIG. 1. The DFT-PBE derived phonon dispersions of graphene. ZA: the out-of-plane acoustic branch, ZO: the out-of-plane optical branch, TA: transverse-acoustic branch, TO: transverse-optical branch, LA: longitudinal-acoustic branch, LO: longitudinal-optical branch. Note that seven phononic Weyl nodes are marked by the pink transparent circles, and the three blue circles are three nodal points on the nodal line formed by the crossing between the lowest out-of-plane optical (ZO) and the highest longitudinal-acoustic (LA) branches.

correlation function [17]. They treat semi-core valence electrons as valence electrons. To obtain the stable phonon spectra, a high accurate optimization of the lattice constants have been performed by minimizing the interionic forces within 0.0001 eV/Å. The cut-off energy for the expansion of the wave function into the plane waves was 550 eV. The Monkhorst-Pack k-meshe (21×21×1) is used for the BZ integrations with a resolution of $2\pi \times 0.01\text{Å}$. By trying various supercells for the calculations of phonon dispersions, it has been found that the $7 \times 7 \times 1$ supercell yielded a high accuracy to provide the most reliable force constants by combining both the VASP and Phonopy code [18]. Of course, we have also computed the phonon spectrum by including the spin-orbital coupling (SOC) effect and the SOC doesn't exhibit any influence on phonon. By using the force constants as hopping parameters, we have built the dynamic matrices to analyze the topological nature. The boundary phonon dispersions have been performed by constructing the chain model and the boundary-edged phonon densities of states have also been obtained by using the iteration Green's function method [19].

We have recalculated the phonon dispersions of graphene in Fig. 1, which is in nice agreement with previous calculations [20–22]. Importantly, we have observed several linear crossings of the phonon bands in Fig. 1. At the K point - the BZ corners, there are two linear crossings of the phonon bands, clearly stemming from the band crossing between the ZA and ZO branches at 15.92 THz and from another band crossing between the LA and LO branches at about 36.36 THz. The former is marked with PW1 and the latter with PW2 in Fig. 1. In addition, we still note that there exist the two types of band crossings between LO and TO branches along Γ -M and Γ -K (Γ -K') paths, as defined as PW3 and PW4, respectively. In

particular, these four crossing points (PW1, PW2, PW3 and PW4) are the isolated points, showing the conical band structure on the q_{xy} plane. The PW1 has the lowest frequency among those four crossings. We have plot the band structure between the ZA and ZO branches on the q_{xy} plane of the BZ in Fig. 2 (a and b) from which the conical structure can be clearly evidenced. Interestingly, the conical shapes of the PW2 and PW3 are very similar to that of the PW1, although their frequencies are different. However, the conical shape of the PW4 highly differs, as its conical structure on the q_{xy} plane is tilted as shown in Fig. 2(c). To identify whether these four PWs exhibit topological nature, we have calculated their Berry curvatures on a 2D q_{xy} plane. It needs to be emphasized that for 2D crystals the Berry curvature only has non-zero value (Ω_{xy}) along q_z direction, whereas Ω_{yz} and Ω_{zx} have to be zero. Here, we have selected PW1 and PW4 as the examples. Figure 2(d and e) shows the Berry curvatures of the ZA/ZO crossing (PW1) at K and K', indicating that their Berry curvatures only have the extremum exactly at K and K' but with the opposite signs and at all other position the Berry curvature is strictly zero. The fact reveals that the PW1 at the K and K' have opposite charges. Furthermore, both PW2 and PW3 show the similar feature to PW1. We have also calculated the Berry curvature of the PW4 on the 2D q_{xy} plane in Fig. 2(f), evidencing the isolated maximum value only at the defined A point along the Γ -K path, whereas the Berry curvature at any other q point is almost zero. Moreover, we have calculated their Berry phases as

$$\gamma_n = \oint_C \mathbf{A}_n(\mathbf{q}) \cdot d\mathbf{l}, \quad (1)$$

where $\mathbf{A}_n(\mathbf{q}) = i\langle u_n(\mathbf{q}) | \nabla_{\mathbf{q}} | u_n(\mathbf{q}) \rangle$ is the Berry connection and $u_n(\mathbf{q})$ is the Bloch wavefunction of n -th band. For this purpose, we have defined a closed circle on the q_{xy} plane centered at the $q = K$ momentum to calculate Berry phase. The radius of the closed circle going around this K point can be selected to be arbitrary large, as long as it does not also cover another K or K' point. Interestingly, the Berry phase for this crossing point PW1 at K is $-\pi$, whereas another crossing point at K' has an opposite Berry phase of π . This fact means that the two crossing points of PW1 at K or K' are topological non-trivial and also proves that the topological property of the band crossings at K or K' are opposite in their chirality. Therefore, these band crossing points, PW1, at K and K' are indeed a pair of phononic Weyl-like nodes with the opposite chirality. Thus, we have also analyzed the Berry phases of the other three crossing points (PW2, PW3 and PW4), revealing that they have the same topological property as PW1 with the value of π or $-\pi$. Therefore, all these four crossing points of PW1, PW2, PW3, and PW4 are phononic Weyl-like points. It needs to be emphasized that the general Weyl point is in the 3D conical shape [23], as already emphasized in many electronic Weyl semimetals [24–55] and several phononic Weyl materials [56–62]. However, given the fact that it is not physically allowed for any 3D shape for graphene due to its single layer structure and the phononic band is spinless, it is reason-

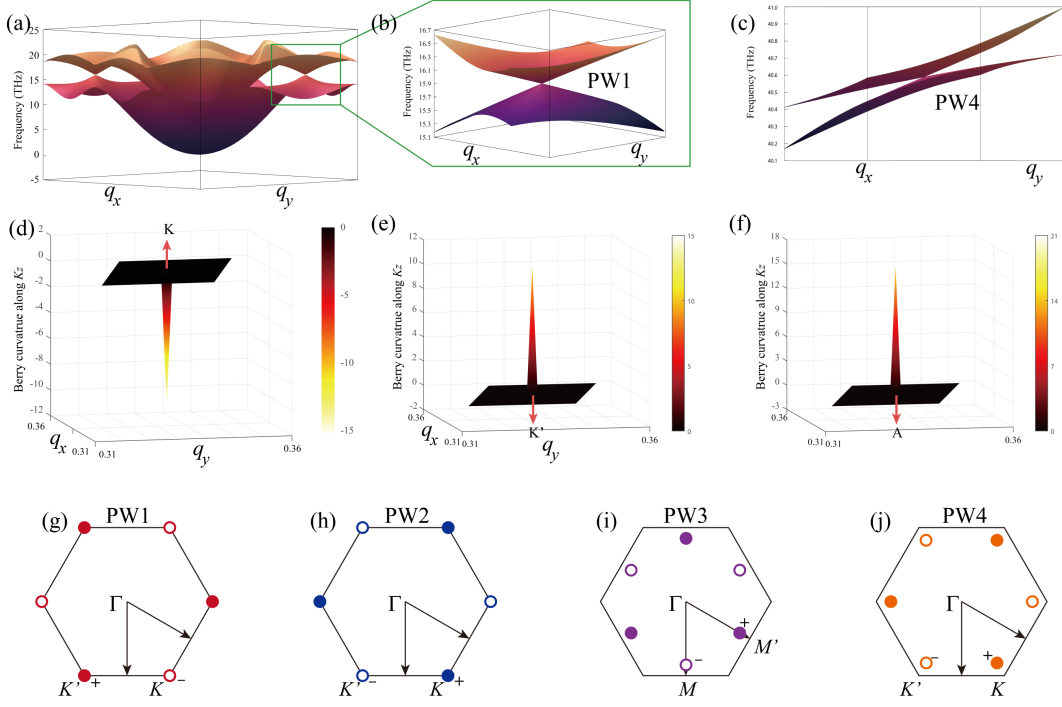


FIG. 2. Weyl-like phonons at K and K' in graphene. Panel (a): The 3D visualization of the DFT-PBE derived phonon ZA and ZO branches of graphene to show the linear crossing, PW1, at the K and K' point in the BZ. Panel (b): The zoom-in 3D visualization of both ZA and ZO branches surrounding the K point of the BZ. Panel (c): The visualized DFT-PBE derived phonon LO and TO branches of graphene to show the linear crossing, PW4, along the Γ and K path in the BZ. Panel (d and e): The derived Berry curvature surrounding the phononic Weyl-like point, PW1, at K (or K') point on the $q_{x,y}$ plane ($q_x = 0.31 - 0.36$; $q_y = 0.31 - 0.36$) of the BZ. Panel (f): The distribution of Berry curvature of the Weyl point, PW4, at the defined A point of the 2D BZ. Panels (g to j): the distribution of the Weyl-like points in the first BZ of graphene, PW1, PW2, PW3 and PW4, respectively.

able to define these crossings as Weyl-like phonons. Given the fact that PW1, PW2 and PW3 exhibit the normal conical shape whereas the PW4 has tilted conical shape, PW1, PW2 and PW3 are the so-called type-I Weyl-like points and PW4 is the typical type-II Weyl-like point. All these Weyl-like nodes obey three-fold rotation symmetry and thus each type of Weyl-like points have three pairs in their 2D first BZ, as illustrated in Fig. 2(g, h, i and j).

We have still noted that at 24 THz the phononic linear band crossings occur between the LA and ZO branches along the Γ - K (or K') and Γ - M directions (Fig. 1). Importantly, these three linear crossing points are not isolated and, instead, they form a closed phononic nodal line (PNL) around Γ point in the BZ. In order to clearly see the shape of the PNL, we have visualized the phonon bands of both ZO and LA branches on the $q_{x,y}$ plane in Fig. 3(a). The specified location of the PNL is shown in the BZ in Fig. 3(b) in which we have used the gap between the ZO and LA branches to obtain the PNL distribution, evidencing the occurrence of the closed black circle centered at the Γ point.

For 2D crystal, the topological non-trivial nature can be observed by the edge states. To elucidate this feature, we have employed the phononic tight-binding model to construct the supercell of a ribbon model (Fig. 3(a)) along different directions and the edge phononic bands are obtained by the trun-

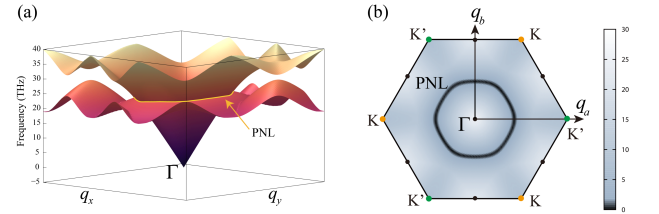


FIG. 3. Panel (a): The 3D visualization of the DFT-PBE derived phonon ZO and LA branches of graphene to show the phononic nodal line surrounding the Γ point in the BZ. Panel (b): The gap between these two ZO/LA branches in the first BZ. The black closed circle represents the PNL on $q_{x,y}$ plane.

cated chain of graphene. Through the Green's function iteration method, the 2D and edge phononic densities of states can be obtained through the imaginary parts of the Green's function. Currently, we have mainly focused on the two representative edge states of the zigzag-edged boundary (the $[100]$ direction in Fig. 4(a)) and of the armchair-edged boundary (the $[1\bar{1}0]$ direction) as shown in supplementary materials [68]. From the phonon dispersions of the zigzag-edged boundary in Fig. 4(b), four distinct topologically protected non-trivial edge phononic states can be observed. In the first, at about 16 THz of the zigzag-edged phononic states a straight-line state

is formed to connect two projected type-I PW1 points with the opposite chirality. To illuminate the edge states, we have analyzed the Bloch modes of a selected point on the edge states. As shown in Fig 4 (b) and (e), the point is marked by the blue circle on the edge states and its coordinate is $q = (0.45, 0.0)\frac{2\pi}{a}$. This two-fold degenerate band originates from the ZA and ZO modes of the pristine phonons of graphene. From the tight binding model, we have analyzed the vibration modes of these two phononic bands on the edge states. As expected, these two edge bands are associated with the out-of-plane vibration modes only along the k_z direction for the edged carbon atoms in Fig. 4(a), which are exactly the same as the ZA and ZO modes correlated with the PW1 Weyl nodes of pristine graphene. In particular, at $q = (0.5, 0.0)\frac{2\pi}{a}$ each of the twofold degenerate phonon edge bands is only contributed by the carbon atoms at the zigzag boundaries. As illustrated in Fig. 4(a), the sharp spatial Bloch modes of those two phononic bands are strictly confined at the zigzag edges. This fact means that the two-fold degenerate edged states only propagate along the edged boundaries. Remarkably, this straight-line phononic edge state has a nearly flat phononic dispersion upon various q momentum from \bar{K} to \bar{K}' , as illustrated in Fig. 4(e). It reveals that the phononic edge states originated from the PW1 Weyl-like points have the nearly zero phonon group velocity (namely, $v(q) \approx 0$) in the phonon one-way transport direction along the zigzag-edged boundary of graphene. This interesting feature of the zigzag-edged narrow ribbon of graphene would have potential application for the emitting of the ultra slow light. Of course, we have also analyzed other points of the phononic edge states, revealing the similar spatial and local properties of vibrations. In the second, for PW2 at 36.36 THz there is a distinct two-fold edge state connecting two PW2-projected points with different chirality as shown in Fig 4(b), which is marked by red and blue lines. At around 41.50 THz, the other phonon edge states can be also visualized to connect type-I PW3 Weyl-like points with the opposite chirality, as shown in Fig. 4(c). In comparison with the edge states induced by PW1 and PW2, the PW3-induced edge states are not only shorter in the q momentum but also exhibit relatively larger dispersions. Moreover, it needs to be emphasized that for PW4 no edge states can be clearly observed because the PW4-induced topologically protected phononic edge states fully overlap with the edge projection from the phonon dispersions of the pristine graphene. In the third, in similarity to the nodal lines in 3D crystals which exhibits non-trivial drumhead-like surface states for BaSn₂, Ca₃P, TiTaSe₂ and TiSi, ZrSiS [63–67] and the phononic Weyl nodal line MgB₂ [60], the existence of PNL of the pristine graphene at 24.38 THz induces the straight-line edge states, simultaneously, with an arc-like going-downwards parabola in its frequencies upon the q momentum, as shown in Fig. 4(d). Moreover, this PNL-induced topologically protected phononic edge states for the armchair-edged boundary of graphene has been further discussed in the supplementary materials [68].

The occurrence of single phononic Weyl-like nodes in the BZ is very important for graphene, which provide an

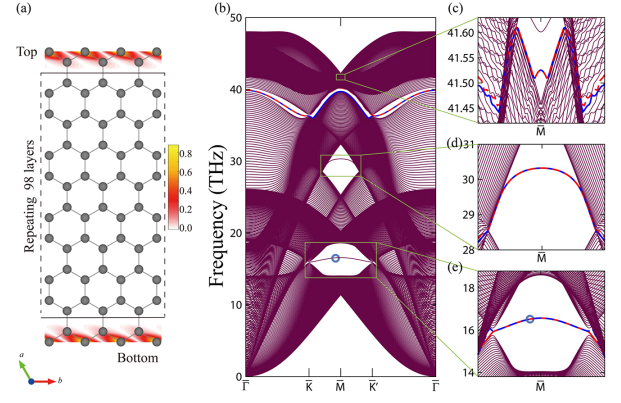


FIG. 4. The phonon dispersions of the zigzag-edged boundaries (along the [100] direction) of graphene. Panel (a): The ribbon model of graphene with the zigzag-edged boundary. Panel (b): The phonon dispersion of the ribbon model derived by the tight-binding calculations along the zigzag-edged high-symmetry paths. Panels (c,d,e): the zoom-in local phonon dispersions connecting to the projection sites of the PW3, PNL and PW1 phonons around the \bar{M} point. Note that we have plot the edge states in Panel (a) on a selected point (as marked by a close circle in panel (b)) of the PW1-induced topologically protected phononic edge dispersion.

ideal platform to study novel topological phononic properties, such as destructive interference and quantum (anomalous/spin) Hall-like topological effects. Firstly, it is clear that the chiral electrons in graphene [69] moving along a closed path have been demonstrated to exhibit a phase change of the two components of the wave function. This fact leads to a new phase, which contributes to the interference processes. In similarity to electron in graphene, the Weyl-like phonons at both K and K' have the opposite chirality for both PW1 and PW2. If phonon traverses such a closed path without being scattered, protected by the PW-induced non-trivial phononic edge states, from a PW at K to the other PW at K' , the Berry phase definitely changes its sign of the amplitude of one path with respect to the time-reversed path[69]. Therefore, these two paths possibly form so-called destructive interference, as accompanied with a suppression of backscattering. As shown in Fig. 4(a) for the robust phononic non-trivial edge states induced by the PW1 along the K to K' path, the phonon destructive interference would be reasonably expected. The similar behaviors would also hold for both PW3 on the $\bar{\Gamma}$ - \bar{M} direction and PW4 along the $\bar{\Gamma}$ - \bar{K} direction. Secondly, it is interesting to emphasize that, as shown in Fig. 2, the Berry curvatures are vanishingly zero throughout the BZ, except for the positions of four pairs of PWs (Fig. 2). At these PWs, the non-zero Berry curvatures (corresponding to the Berry phase of π and $-\pi$) appear, associated with PW1, PW2, PW3, and PW4 (Fig. 2). They can be indeed viewed as magnetic field in momentum space, accordingly leading to the possible occurrence of the phononic quantum (anomalous/spin) Hall-like topological effects.

Unexpectedly, through first-principles calculations and

modeling analysis we have revealed the existence of intrinsic topological Weyl-like and PNL phonons in pristine graphene, as accompanied with the robust appearance of the topologically protected one-way phononic edge states. Given the fact that many novel physical properties are related with phonons, graphene would be an ideal case to elucidate fundamental physical phenomena related with topological phonons, possibly including heat conduction, electrical resistance, and phonon wave-guides, as well as electron-phonon coupling effects for superconductivity.

Acknowledgments Work was supported by the National Science Fund for Distinguished Young Scholars (No. 51725103) and by the National Natural Science Foundation of China (Grant No. 51671193). All calculations have been performed on the high-performance computational cluster in the Shenyang National University Science and Technology Park.

* xingqiu.chen@imr.ac.cn

- [1] C. L. Kane and E. J. Mele, Quantum Spin Hall Effect in Graphene, *Phys. Rev. Lett.* **95**, 226801 (2005).
- [2] B. A. Bernevig, T. L. Hughes, S.-C. Zhang, Quantum spin Hall effect and topological phase transition in HgTe quantum wells, *Science* **314**, 1757 (2006).
- [3] M. König, S. Wiedmann, C. Brüne, A. Roth, H. Buhmann, L. W. Molenkamp, X.-L. Qi, S.-C. Zhang, Quantum spin Hall insulator state in HgTe quantum wells, *Science* **318**, 766 (2007).
- [4] L. Zhang, J. Ren, J.-S. Wang, and B. Li, Topological Nature of the Phonon Hall Effect, *Phys. Rev. Lett.* **105**, 225901 (2010).
- [5] D. Jin, T. Christensen, M. Soljacic, N. X. Fang, L. Lu, and X. Zhang, *Infrared Topological Plasmons in Graphene*, *Phys. Rev. Lett.* **118**, 245301 (2017).
- [6] E. Prodan, and C. Prodan, Topological Phonon Modes and Their Role in Dynamic Instability of Microtubules, *Phys. Rev. Lett.* **103**, 248101 (2009).
- [7] P. Wang, L. Lu, and K. Bertoldi, Topological Phononic Crystals with One-Way Elastic Edge Waves, *Phys. Rev. Lett.* **115**, 104302 (2015).
- [8] Y. Z. Liu, C.-S. Lian, Y. Li, Y. Xu, and W. H. Duan, Pseudospins and Topological Effects of Phonons in a Kekulé Lattice, *Phys. Rev. Lett.* **119**, 255901 (2017).
- [9] P. Hohenberg and W. Kohn, Inhomogeneous Electron Gas, *Phys. Rev.* **136**, B864 (1964).
- [10] W. Kohn, and L. J. Sham, Self-Consistent Equations Including Exchange and Correlation Effects, *Phys. Rev.* **140**, A1133 (1965).
- [11] S. Baroni, S. D. Gironcoli, A. D. Corso, and P. Giannozzi, Phonons and related crystal properties from density-functional perturbation theory, *Rev. Mod. Phys.* **73**, 515 (2001).
- [12] G. Kresse and J. Hafner, Ab initio molecular dynamics for liquid metals, *Phys. Rev. B* **47**, 558 (1993).
- [13] G. Kresse, and J. Hafner, Ab initio molecular-dynamics simulation of the liquid-metal amorphous-semiconductor transition in germanium, *Phys. Rev. B* **49**, 14251 (1994).
- [14] G. Kresse and J. Furthmüller, Efficiency of ab-initio total energy calculations for metals and semiconductors using a plane-wave basis set, *Comput. Mater. Sci.* **6**, 15 (1996).
- [15] P. E. Blöchl, Projector augmented-wave method, *Phys. Rev. B* **50**, 17953 (1994).
- [16] G. Kresse and D. Joubert, From ultrasoft pseudopotentials to the projector augmented-wave method, *Phys. Rev. B* **59**, 1758 (1999).
- [17] J. P. Perdew, K. Burke, and M. Ernzerhof, Generalized Gradient Approximation Made Simple, *Phys. Rev. Lett.* **77**, 3865 (1996).
- [18] L. Chaput, A. Togo, I. Tanaka, and G. Hug, Phonon-phonon interactions in transition metals, *Phys. Rev. B* **84**, 094302 (2011).
- [19] M. P. Sancho, J. M. Sancho, and J. Rubio, Highly convergent schemes for the calculation of bulk and surface Green functions, *J. Phys. F: Met. Phys.* **15**, 851 (1985).
- [20] N. Mounet and N. Marzari, First-principles determination of the structural, vibrational and thermodynamic properties of diamond, graphite, and derivatives, *Phys. Rev. B* **71**, 205214 (2005).
- [21] N. Bonini, M. Lazzeri, N. Marzari, and F. Mauri, Phonon Anharmonicities in Graphite and Graphene, *Phys. Rev. Lett.* **99**, 176802 (2007).
- [22] D.L. Nika, E. P. Pokatilov, A. S. Askerov and A. A. Balandin, Phonon thermal conduction in graphene: Role of Umklapp and edge roughness scattering, *Phys. Rev. B* **79**, 155413 (2009).
- [23] H. Weyl, Elektron und Gravitation. I, *Z. Phys.* **56**, 330 (1929).
- [24] X. Wan, A. M. Turner, A. Vishwanath, and S. Y. Savrasov, Topological semimetal and Fermi-arc surface states in the electronic structure of pyrochlore iridates, *Phys. Rev. B* **83**, 205101 (2011).
- [25] S.-M. Huang, X.-Y. Xu, I. Belopolski, C.-C. Lee, G. Q. Chang, B. K. Wang, N. Alidoust, G. Bian, M. Neupane, C. L. Zhang, S. Jia, A. Bansil, H. Lin, and M. Z. Hasan, A Weyl Fermion semimetal with surface Fermi arcs in the transition metal mononitride TaAs class, *Nature Commun.* **6**, 7373 (2015).
- [26] H. M. Weng, C. Fang, Z. Fang, B. A. Bernevig, and X. Dai, Weyl Semimetal Phase in Noncentrosymmetric Transition-Metal Monophosphides, *Phys. Rev. X* **5**, 011029 (2015).
- [27] S.-Y. Xu, *et al.*, Discovery of a Weyl fermion state with Fermi arcs in niobium arsenide, *Nature Phys.* **11**, 748 (2015).
- [28] S.-Y. Xu, *et al.*, Discovery of a Weyl fermion semimetal and topological Fermi arcs, *Science* **349**, 613 (2015).
- [29] A. A. Soluyanov, D. Gresch, Z. Wang, Q. S. Wu, M. Troyer, X. Dai, and B. A. Bernevig, Type-II Weyl semimetals, *Nature* **527**, 495 (2015).
- [30] Y. Sun, S.-C. Wu, M. N. Ali, C. Felser, and B. H. Yan, Prediction of Weyl semimetal in orthorhombic MoTe₂, *Phys. Rev. B* **92**, 161107(R) (2015).
- [31] R. Yu, Q. S. Wu, Z. Fang, and H. M. Weng, From Nodal Chain Semimetal to Weyl Semimetal in HfC, *Phys. Rev. Lett.* **119**, 036401 (2017).
- [32] C. Fang, M. J. Gilbert, X. Dai, and B. A. Bernevig, Multi-Weyl Topological Semimetals Stabilized by Point Group Symmetry, *Phys. Rev. Lett.* **108**, 266802 (2012).
- [33] T. Dubček, C. J. Kennedy, L. Lu, W. Ketterle, M. Soljačić, and H. Buljan, Weyl Points in Three-Dimensional Optical Lattices: Synthetic Magnetic Monopoles in Momentum Space, *Phys. Rev. Lett.* **114**, 225301 (2015).
- [34] L. Lu, J. D. Joannopoulos, and M. Soljačić, Topological photonics, *Nature Photon.* **8**, 821 (2014).
- [35] L. Lu, L. Fu, J. D. Joannopoulos, and M. Soljačić, Weyl points and line nodes in gyroid photonic crystals, *Nature Photon.* **7**, 294 (2013).
- [36] Q. Lin, M. Xiao, L. Yuan, and S. Fan, Photonic Weyl point in a two-dimensional resonator lattice with a synthetic frequency dimension, *Nature Commun.* **7**, 13731 (2016).
- [37] W.-J. Chen, M. Xiao and C. T. Chan Photonic crystals possess-

- ing multiple Weyl points and the experimental observation of robust surface states, *Nature Commun.* **7**, 13038 (2016)
- [38] J. Noh, S. Huang, D. Leykam, Y. D. Chong, K. P. Chen, and M. C. Rechtsman, Experimental observation of optical Weyl points and Fermi arc-like surface states, *Nature Phys.* **13**, 611 (2017).
- [39] H. He, C. Qiu, L. Ye, X. Cai, X. Fan, M. Ke, F. Zhang, Z. Liu, Topological negative refraction of surface acoustic waves in a Weyl phononic crystal, *Nature*, **560**, 61 (2018).
- [40] M. Xiao, W.-J. Chen, W.-Y. He, and C. T. Chan, Synthetic gauge flux and Weyl points in acoustic systems, *Nature Phys.* **11**, 920 (2015).
- [41] Z. Yang, F. Gao, X. Shi, X. Lin, Z. Gao, Y. Chong, and B. Zhang, Topological Acoustics, *Phys. Rev. Lett.* **114**, 114301 (2015).
- [42] I. Belopolski, *et al.*, Criteria for Directly Detecting Topological Fermi Arcs in Weyl Semimetals, *Phys. Rev. Lett.* **116**, 066802 (2016).
- [43] J. Ahn, and B.-J. Yang, Unconventional Topological Phase Transition in Two-Dimensional Systems with Space-Time Inversion Symmetry, *Phys. Rev. Lett.* **118**, 156401 (2017).
- [44] Y. Xu, F. Zhang, and C. Zhang, Structured Weyl Points in Spin-Orbit Coupled Fermionic Superfluids, *Phys. Rev. Lett.* **115**, 265304 (2015).
- [45] D. Z. Rocklin, B. G. Chen, M. Falk, V. Vitelli, and T. C. Lubensky, Mechanical Weyl Modes in Topological Maxwell Lattices, *Phys. Rev. Lett.* **116**, 135503 (2016).
- [46] Z. Yan, and Z. Wang, Tunable Weyl Points in Periodically Driven Nodal Line Semimetals, *Phys. Rev. Lett.* **117**, 087402 (2016).
- [47] J. Ruan, S.-K. Jian, H. Yao, H. Zhang, S.-C. Zhang and D. Xing, Symmetry-protected ideal Weyl semimetal in HgTe-class materials, *Nature Commun.* **7**, 11136 (2016).
- [48] Z. Gao, M. Hua, H. Zhang, and X. Zhang, Classification of stable Dirac and Weyl semimetals with reflection and rotational symmetry, *Phys. Rev. B* **93**, 205109 (2016).
- [49] L. Lu, Z. Wang, D. Ye, L. Ran, L. Fu, J. D. Joannopoulos, M. Soljačić, Experimental observation of Weyl points, *Science* **349**, 622 (2015).
- [50] B. Q. Lv, Z.-L. Feng, Q.-N. Xu, X. Gao, J.-Z. Ma, L.-Y. Kong, P. Richard, Y.-B. Huang, V. N. Strocov, C. Fang, H.-M. Weng, Y.-G. Shi, T. Qian and H. Ding, Observation of three-component fermions in the topological semimetal molybdenum phosphide, *Nature* **546**, 627 (2017).
- [51] J. Gooth, A. C. Niemann, T. Meng, A. G. Grushin, K. Landsteiner, B. Gotsmann, F. Menges, M. Schmidt, C. Shekhar, V. Süß, R. Hühne, Bernd Rellinghaus, C. Felser, B. Yan and K. Nielsch, Experimental signatures of the mixed axial-gravitational anomaly in the Weyl semimetal NbP, *Nature* **547**, 324 (2017).
- [52] H. Inoue, A. Gyenis, Z. Wang, J. Li, S. Woo Oh, S. Jiang, N. Ni, B. A. Bernevig, A. Yazdani, Quasiparticle interference of the Fermi arcs and surface-bulk connectivity of a Weyl semimetal, *Science* **351**, 1184 (2016).
- [53] H. M. Weng, C. Fang, Z. Fang, and X. Dai, Coexistence of Weyl fermion and massless triply degenerate nodal points, *Phys. Rev. B* **94**, 165201 (2016).
- [54] H. M. Weng, C. Fang, Z. Fang, and X. Dai, Topological semimetals with triply degenerate nodal points in θ -phase tantalum nitride, *Phys. Rev. B* **93**, 241202(R) (2016).
- [55] S. Wang, B.-C. Lin, A.-Q. Wang, D.-P. Yu, and Z.-M. Liao, Quantum transport in Dirac and Weyl semimetals: a review, *Advances in Physics: X*, **2**, 518 (2017)
- [56] O. Stenull, C. L. Kane, and T. C. Lubensky, Topological Phonons and Weyl Lines in Three Dimensions, *Phys. Rev. Lett.* **117**, 068001 (2016).
- [57] T. T. Zhang, Z. D. Song, A. Alexandradinata, H. M. Weng, C. Fang, L. Lu, and Z. Fang, Double-Weyl phonons in transition-metal monosilicides, *Phys. Rev. Lett.* **120**, 016401 (2018)
- [58] Q. Xie, J. X. Li, S. Ullah, R. H. Li, L. Wang, D. Z. Li, Y. Y. Li, S. Yunoki, and X.-Q. Chen, Phononic Weyl points and one-way topologically protected nontrivial phononic surface arc states in noncentrosymmetric WC-type materials, *Phys. Rev. B* **99**, 174306 (2019)
- [59] H. Miao, T. T. Zhang, L. Wang, D. Meyers, A. H. Said, Y. L. Wang, Y. G. Shi, H. M. Weng, Z. Fang, and M. P. M. Dean, Observation of Double Weyl Phonons in Parity-Breaking FeSi, *Phys. Rev. Lett.* **121**, 035302 (2018)
- [60] Q. Xie, J. X. Li, M. Liu, L. Wang, D. Z. Li, Y. Y. Li, and X.-Q. Chen, Phononic Weyl Nodal Straight Lines in High-Temperature Superconductor MgB_2 , *arXiv:1801.04048*
- [61] S. Singh, Q. S. Wu, C. M. Yue, A. H. Romero, and A. A. Soluyanov, Topological phonons and thermoelectricity in triple-point metals, *Phys. Rev. Mater.* **2**, 114204 (2018)
- [62] J. X. Li, Q. Xie, S. Ullah, R. H. Li, H. Ma, D. Z. Li, Y. Y. Li, and X.-Q. Chen, Coexistent three-component and two-component Weyl phonons in TiS, ZrSe, and HfTe, *Phys. Rev. B* **97**, 054305 (2018)
- [63] H. Huang, J. P. Liu, D. Vanderbilt, W. H. Duan, Topological nodal-line semimetals in alkaline-earth stannides, germanides, and silicides, *Phys. Rev. B* **93**, 201114 (2016)
- [64] M. Neupane, I. Belopolski, M. M. Hosen, D. S. Sanchez, R. Sankar, M. Szlawaska, S.-Y. Xu, K. Dimitri, N. Dhakal, P. Maldonado, P. M. Oppeneer, D. Kaczorowski, F. Chou, M. Z. Hasan, and T. Durakiewicz, Observation of topological nodal fermion semimetal phase in ZrSiS *Phys. Rev. B* **93**, 201104(R) (2016)
- [65] J. X. Li, H. Ma, Q. Xie, S. B. Feng, S. Ullah, R. Li, J. Dong, D. Z. Li, Y. Y. Li, and X.-Q. Chen, Topological quantum catalyst: Dirac nodal line states and a potential catalyst of hydrogen evolution in the TiSi-family, *Sci. China Mater.* **61**, 23 (2018).
- [66] Y.-H. Chan, C.-K. Chiu, M. Y. Chou, A. P. Schnyder, Ca_3P_2 and other topological semimetals with line nodes and drumhead surface states, *Phys. Rev. B*, **93**, 205132, (2016)
- [67] G. Bian, T.-R. Chang, H. Zheng, S. Velury, S.-Y. Xu, T. Neupert, C.-K. Chiu, S.-M. Huang, D. S. Sanchez, I. Belopolski, N. Alidoust, P.-J. Chen, G. Chang, A. Bansil, H.-T. Jeng, H. Lin, and M. Z. Hasan, Drumhead surface states and topological nodal-line fermions in TiTaSe_2 , *Phys. Rev. B*, **93**, 121113 (2016)
- [68] The supplementary materials contain the discussions of the topologically protected non-trivial phononic edge states of the armchair-edged boundaries of graphene.
- [69] A. H. Castro Neto, F. Guinea, N. M. R. Peres, K. S. Novoselov, and A. K. Geim, The electronic properties of graphene, *Rev. Mod. Phys.*, **81**, 109 (2009)